

Heterogeneity in Epoxy Nanocomposites Initiates Crazeing: Significant Improvements in Fatigue Resistance and Toughening**

Wei Zhang, Itri Srivastava, Yue-Feng Zhu, Catalin R. Picu, and Nikhil A. Koratkar*

Crazeing is a failure mode of bulk polymers and occurs under predominant uniaxial tensile load when the bulk eventually forms denser ligaments (or fibrils) while preserving its continuity.^[1–2] The bridging of cracks by such fibrils is an important mechanism for energy dissipation and toughening in thermoplastic polymers. However, craze phenomena are not observed^[3–5] in thermosetting polymers such as epoxies due to the high crosslinking density of the epoxy chains, which limits molecular mobility and inhibits craze fibril formation. Such thermosetting epoxies typically display a brittle failure.^[6–7] We demonstrate here that thermosetting epoxies reinforced with amido-amine-functionalized multiwalled carbon nanotubes (A-MWNTs) exhibit crazeing. We show order of magnitude reduction in fatigue crack growth rates as a result of the crazeing. The fracture toughness and ductility of the brittle epoxy is also significantly enhanced by the crazeing. Importantly these enhancements in fatigue resistance and toughness are achieved without any softening of the material. In fact, the Young's modulus of the nanocomposite is $\approx 30\%$ greater and the average hardness of the nanocomposite is $\approx 45\%$ higher than the baseline (pristine) epoxy. We show that this effect is related to heterogeneous curing of the epoxy, which results in localized pockets of uncrosslinked epoxy that are trapped (or frozen) at the nanotube–matrix interfaces. Under mechanical loading, these localized regions of high molecular mobility can evolve (or coalesce) to generate conditions that are favorable for crazeing. Recently, in a very interesting study,^[8] crazeing has been reported for a poly(lactide-co-glycolide) thermosetting polymer filled with surface-modified clay nanoparticles. However to the best of our

knowledge this is the first report of crazeing in a thermosetting epoxy. Given the widespread use of epoxies in structural applications, the over ten-fold improvement in fatigue resistance reported here (coupled with enhanced stiffness, strength, and hardness) is expected to translate into significant practical applications of these nanocomposite epoxies.

The traditional view of toughening in fiber-reinforced epoxy composites^[9–10] is that the crack interfaces are bridged by the fiber additives and not by epoxy fibrils (i.e., crazeing is not taking place). This is consistent with our prior experiments^[11–12] with pristine (i.e., non-functionalized) MWNTs dispersed in epoxy matrices. However, the above situation changes drastically when A-MWNTs are used as the nanofiller. The procedures that were used to functionalize the pristine MWNTs with amido-amine ($-\text{NHCH}_2\text{CH}_2\text{NH}_2$) groups (Figure 1a) and disperse the A-MWNTs in a bisphenol-A based epoxy^[13] are described later and in the Supporting Information. The presence of amido-amine groups on the MWNTs was confirmed using IR spectroscopy (see Supporting Information). The spatial density of the functional groups was estimated based on mass loss of various samples in thermogravimetric analysis (TGA) and atomic weights of carbon and other groups. For the A-MWNTs used in our tests, TGA analysis revealed the presence of one amido-amine group for every ≈ 560 carbon atoms. An artifact of the functionalization was a significant shortening of the tube length due to oxidation in the acid medium; the average length of the A-MWNTs was $\approx 1 \mu\text{m}$ (Figure 1a) in comparison to about $2 \mu\text{m}$ prior to functionalization. The diameter (Figure 1a) of the A-MWNTs was $\approx 30 \text{ nm}$. The dispersion quality of the MWNTs and A-MWNTs in the epoxy matrix was quite similar as indicated by scanning electron microscopy (SEM) characterization of freeze-fractured samples (see Supporting Information).

Fatigue crack propagation tests showing crack propagation rate versus stress intensity factor amplitude are shown in Figure 1b for the baseline epoxy, epoxy with 0.25 wt% MWNTs, and epoxy with 0.25 wt% A-MWNTs. The fatigue tests were conducted using a MTS-858 system following ASTM standard E647-05 (sample geometry provided in Supporting Information). From the results we see an over ten-fold reduction in the crack growth rate for the A-MWNT/epoxy sample compared to the baseline epoxy over the full range of stress intensity factor amplitudes. In contrast, the MWNT/epoxy composite shows good fatigue suppression performance only at low values of the stress intensity amplitude and its performance rapidly degrades as the

[*] Prof. N. A. Koratkar, W. Zhang, I. Srivastava, Prof. C. R. Picu
Department Mechanical, Aerospace and Nuclear Engineering
Rensselaer Polytechnic Institute
Troy, NY 12180 (USA)
E-mail: koratn@rpi.edu

Prof. Y.-F. Zhu
Department of Mechanical Engineering
Tsinghua University
Beijing 100084 (China)

[**] NAK acknowledges funding support from the US Army under agreement No. W911W6-06-2-0008 and by the US National Science Foundation (Award No. CMS-0347604).

Supporting Information is available on the WWW under <http://www.small-journal.com> or from the author.

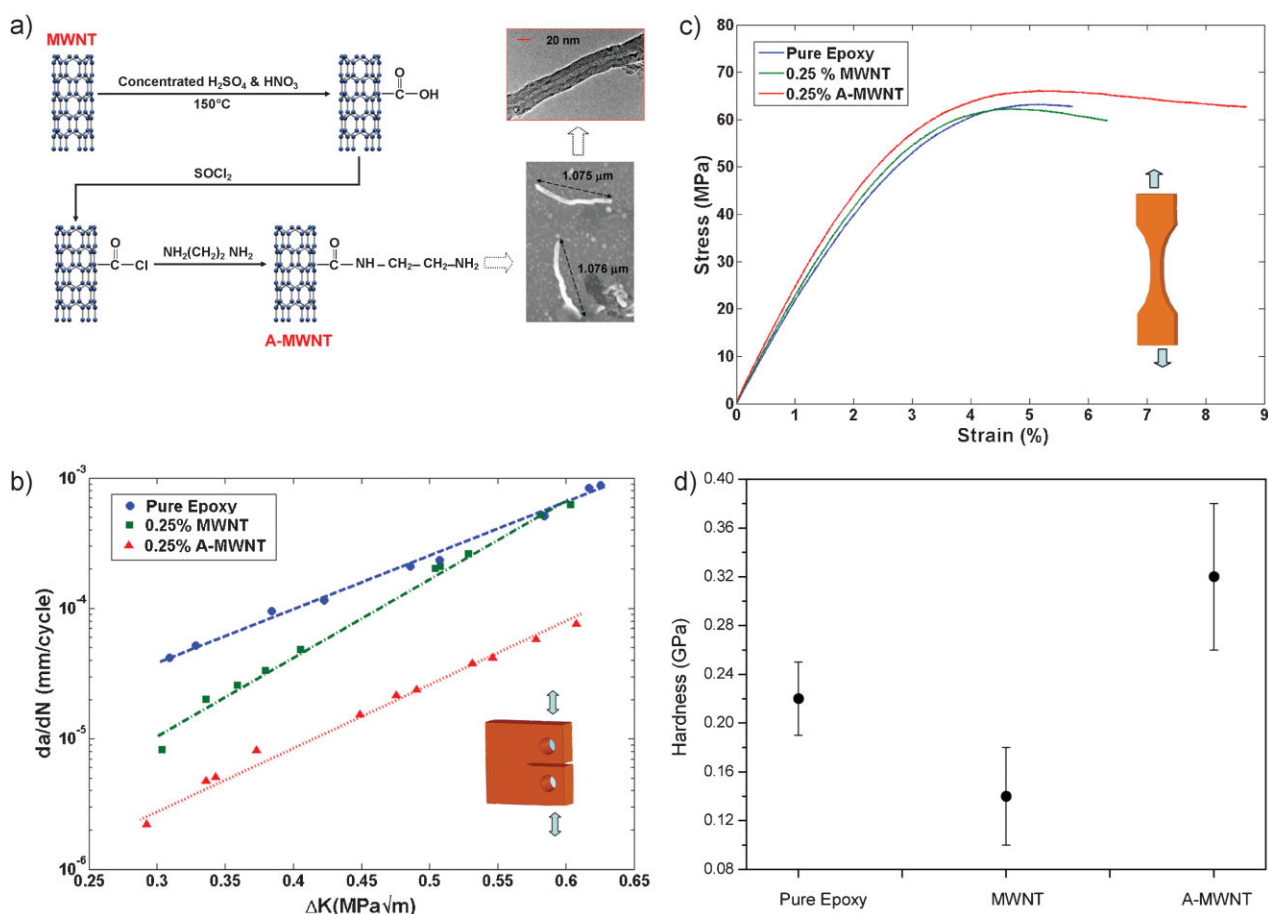


Figure 1. Characterization of mechanical and fatigue properties of the nanocomposite and baseline epoxy. a) The left schematic shows a representation of the functionalization process and the A-MWNT structure. The right SEM image shows that the average length of A-MWNTs is $\approx 1 \mu m$; the A-MWNTs were dispersed in acetone and deposited on a silicon wafer for imaging. The TEM image (top) indicates that the A-MWNT diameter is $\approx 30 nm$. b) Fatigue crack propagation tests showing crack growth rate (da/dN) plotted as a function of the stress intensity factor amplitude (ΔK). The inset shows a schematic of the compact tension samples used in the testing. c) Stress–strain response under static tensile load for the A-MWNT/epoxy, MWNT/epoxy, and baseline (pristine) epoxy samples. The inset shows a schematic of the dog-bone-shaped test coupons used in the testing. d) Nanoindentation measurements of average hardness for the various samples.

amplitude is increased. This behavior for the MWNT/epoxy system is expected and corroborates well with existing models^[11–12] for fiber (MWNT) pull-out in the wake of a propagating crack. These models predict such degradation due to shrinkage of the fiber-bridging zone in the wake of the crack tip at the higher stress intensity factors. What is surprising is that for the A-MWNT/epoxy sample this behavior is not observed. The ten-fold reduction in crack growth rates are maintained across the full range of stress intensity factors. Traditional models based on crack bridging and frictional pull-out^[1,2,14–16] of MWNT fibers cannot explain these observations.

In addition to the cyclic crack propagation tests, we also performed static tensile loading tests for dog-bone-shaped coupons to measure the strain-to-break and static Mode-I crack opening tests on compact tension samples to measure the fracture toughness. The A-MWNT samples show $\approx 60\%$ increase in the strain-to-break with respect to the baseline epoxy compared to only 13% improvement for the MWNT/epoxy samples (Figure 1c). The measured fracture toughness (K_{Ic}) of the A-MWNT samples was $\approx 1.68 MPa \sqrt{m}$ compared

to $1.19 MPa \sqrt{m}$ for the MWNT-epoxy samples and $1.07 MPa \sqrt{m}$ for the baseline epoxy (see Supporting Information). The Young's modulus (Figure 1c) of the A-MWNT/epoxy nanocomposite ($\approx 3.43 GPa$) was $\approx 30\%$ greater than the baseline epoxy ($\approx 2.64 GPa$). We also measured the hardness of the various samples by using a NanoTest 550 Nanoindenter from Micromaterials Inc. We observed that the average hardness (Figure 1d) of the A-MWNT/epoxy nanocomposite ($\approx 0.32 GPa$) was $\approx 45\%$ higher than the baseline epoxy ($\approx 0.22 GPa$); there were significant spatial fluctuations in the hardness values as indicated by the large error bars. Thus the addition of A-MWNT fillers has significantly enhanced the toughness and fatigue resistance of the epoxy, while at the same time enhancing the stiffness, strength, and hardness of the baseline epoxy. The MWNT/epoxy and pure epoxy samples show comparable hardness given the relatively large fluctuations (Figure 1d) in the hardness response.

The fatigue crack propagation results in Figure 1b indicate that a fundamental change in the material response has occurred due to the addition of the A-MWNT fillers. To gain insight into the reasons for this, SEM analysis of the fracture

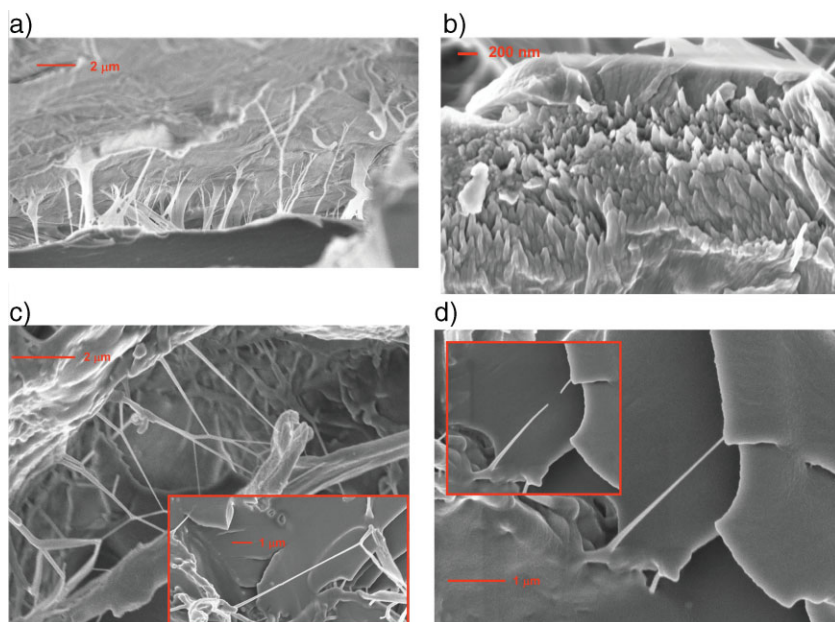


Figure 2. Fractography analysis for the A-MWNT/epoxy nanocomposite. a) SEM micrographs showing crack bridging. The diameter of bridging fibrils is in the 100–1000-nm range. b) SEM micrograph showing dimples that form on the surface after breakage of the bridging fibrils. c) SEM image of stretched out fibrils. The inset shows that the fibrils are up to 10-fold longer than A-MWNTs and are much thicker at the ends compared to the middle portion of the fiber. d) SEM image of fibril before heating. The inset shows the same fibril imaged after heating to 100 °C. The fibril breaks under the thermal loading.

surface of the A-MWNT/epoxy samples was performed. We observed that the cracks are bridged by fibers as seen in the SEM image of Figure 2a. However the diameter of the bridging fibers ranges from about 100 nm to 1 μm. Given that the diameter of an individual A-MWNT is ≈30 nm (Figure 1a), these bridging fibers cannot be A-MWNTs. Moreover the length of the bridging fibrils is several times larger than the A-MWNT length (≈1 μm; Figure 1a). We also observe that for large crack opening displacement the fibrils break and then shrink to form dimples (Figure 2b), suggesting that these bridging fibrils are composed of the epoxy. An interconnected network of stretched out fibrils is shown in Figure 2c. The inset shows an individual fibril that is ≈10 μm in length; the diameter of the fibril is significantly thinner in the middle than at the ends. Given that the length of an individual A-MWNT is ≈1 μm, it would not be feasible for the nanotube to stretch to ten times its original length. It would therefore appear that these bridging fibers are in fact epoxy fibrils that are drawn out in uniaxial tension normal to the crack plane, similar to a craze. To further investigate this we heated the sample to ≈100 °C and then reimaged the sample under SEM. Several of the bridging fibers were observed to break due to the elevated temperatures (Figure 2d), which is expected if these are epoxy fibrils. In fact by locally heating individual fibrils using the electron beam of the SEM (power <3 μW) we were able to rapidly break the fibrils, confirming that the bridging fibers were not high-melting-point MWNTs but fibrils composed of the epoxy. Therefore in our system, the A-MWNTs are initiating the formation of the epoxy craze fibrils and the energy dissipation is due to the pulling and plastic deformation

of the fibril. As a consequence, a model based on frictional pull-out of MWNTs is not appropriate here. Instead we consider a force-displacement function for the stretch of a single fibril (see Supporting Information) of the type proposed by Erdogan and Joseph.^[16] Using this model, the crack growth rate for the nanocomposite (under steady state conditions) can be expressed as

$$\frac{da}{dN} = C \left(\frac{\Delta K}{q} \right)^m \quad (1)$$

where da/dN is the rate of crack growth, a is the crack length, N is the number of cycles of fatigue, m is a constant, C is a constant, ΔK is the stress intensity factor amplitude (for the baseline epoxy), and q is the ratio of the effective stress intensity factor for the crack without fibrils to that of the same crack with fibrils. From Equation 1 it is clear that the rate of crack growth in the A-MWNT/epoxy composite is smaller (in a $\log_{10} da/dN$ vs. ΔK plot) than in the pure epoxy by a factor $-m \log_{10} q$. The experimental data (Figure 1b) suggests that the difference in $\log_{10} da/dN$ between the neat epoxy and the A-MWNT/epoxy composite

is -1 , so $-m \log_{10} q = -1$, which gives $q = 1.93$. Using Erdogan and Joseph's solution,^[16] one can show that $q = 1.93$, provided that the parameter

$$A = \frac{K_{Ic}^{epoxy}}{\bar{\sigma} \sqrt{\pi a_c}} = 0.8 \quad (2)$$

where $\bar{\sigma}$ is the bridging stress generated by crazing, a_c is the length of the bridging zone, and K_{Ic}^{epoxy} is the fracture toughness of the baseline epoxy. The above analysis indicates that crack bridging models based on crazing can qualitatively explain the trends for the A-MWNT/epoxy crack growth observed in our experiments (Figure 1b).

We also considered other possible mechanisms for energy dissipation such as crack deflection and crack pinning.^[1–2] To investigate whether crack deflection is playing a role, we used a Dektak Surface Profiler (from VEECO) to obtain the roughness of the fracture surface for the different samples. The results of the surface scans indicated that the average surface roughness of the A-MWNTs is ≈20% greater than the baseline epoxy. This suggests that in addition to the crack-bridging mechanism discussed above, crack deflection also contributes to the observed toughening. Fractography analysis however did not reveal any evidence of crack pinning.

Crazing is typically associated^[17–18] with the development of a uniaxial stress state in the material and with sufficient molecular mobility. Molecular mobility, which would allow molecules to align in the stretch direction, is favored either by bond breaking or by the lack of (or reduced) crosslinking. Heterogeneous epoxy crosslinking near nanofillers could

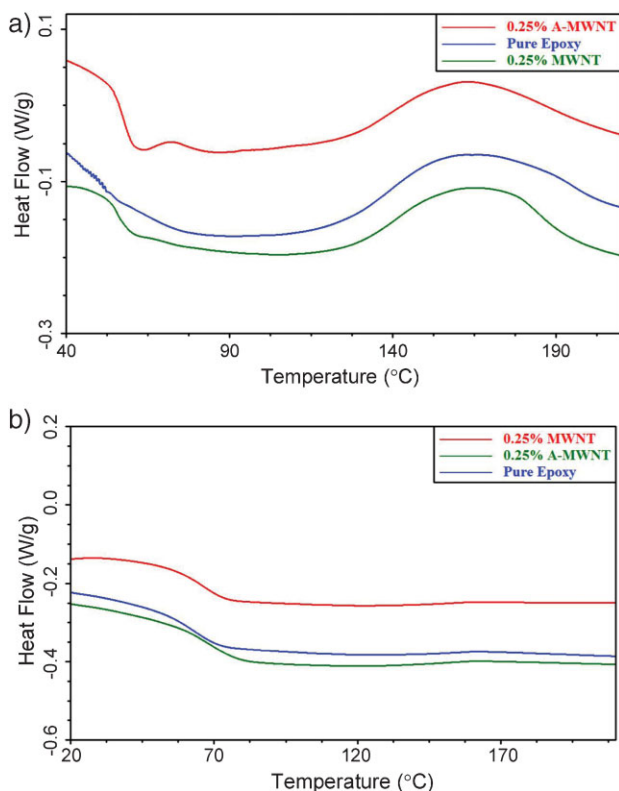


Figure 3. Heterogeneity in curing for the nanocomposite. a) DSC scan showing heat flow versus temperature for the A-MWNT/epoxy, MWNT/epoxy, and baseline epoxy samples. The data are from the initial DSC scan; the exothermic peaks in the response indicate the presence of residual uncured epoxy. b) Subsequent DSC scan on the same samples. No exothermic peaks are observed for this case.

generate such regions of high molecular mobility and spatial fluctuations (variability) in material properties. To investigate this we performed differential scanning calorimetry (DSC) characterization of the various samples. The result of the initial DSC run is shown in Figure 3a. The data indicate a clear exothermic peak for the A-MWNT/epoxy sample at $\approx 70^\circ\text{C}$. No such exothermic peaks are observed for the pure epoxy and MWNT/epoxy samples. The second exothermic peak observed at $\approx 160^\circ\text{C}$ is also a curing peak and is observed for all three samples. The area under this peak is indicative of the residual uncured epoxy in the samples. This area is measured as 68.2 J g^{-1} for the A-MWNT/epoxy compared to only 32.6 J g^{-1} for the MWNT/epoxy and 42.3 J g^{-1} for the baseline epoxy sample. The results of the subsequent DSC run on the same samples are shown in Figure 3b. No exothermic peaks are observed in the second DSC run. The measured glass transition temperatures from the second DSC run for the A-MWNT/epoxy, MWNT/epoxy, and the pure epoxy samples are similar ($\approx 66^\circ\text{C}$).

The exothermic peak (at $\approx 70^\circ\text{C}$) that is unique to the A-MWNT/epoxy composite and the increased area under the curing peak at $\approx 160^\circ\text{C}$ for the A-MWNT/epoxy system suggests that a significant amount of unreacted epoxy is kinetically trapped in the crosslinked matrix structure that is formed at the A-MWNT/epoxy interface. Such local hetero-

geneity in the curing may be caused by a variety of factors such as, for example, the fact that the chemistry may be modified locally due to the presence of amido-amine groups. Epoxy chain alignment, which is known to influence the crosslinking density, may also be modified locally^[19–20] due to presence of these functional groups. Heterogeneous crosslinking results in localized pockets of enhanced molecular mobility; the correlated evolution of such contiguous mobile regions under mechanical loading can initiate crazing as observed in our experiments. It should be noted that the heterogeneities that we report here are localized to the nanotube–matrix interfaces since we do not observe any reduction in the global (macroscale) stiffness, hardness, or strength of the epoxy. In fact, the measured Young's modulus of the A-MWNT/epoxy composite is $\approx 30\%$ greater and its averaged hardness is $\approx 45\%$ higher than the baseline epoxy.

Experimental Section

The MWNTs used in this study were prepared in-house by a conventional chemical vapor deposition method.^[21] Raman spectra for the MWNTs are provided in the Supporting Information. The procedure used to functionalize the MWNTs (Figure 1a) consists of two parts. In the first step MWNTs are oxidized and carboxyl groups ($-\text{COOH}$) are grafted^[22] on the surface of the MWNT. In the second step, thionyl chloride reacts with the carboxyl groups resulting in $-\text{COCl}$. Then 1,2-ethylenediamine reacts with $-\text{COCl}$, producing $-\text{NHCH}_2\text{CH}_2\text{NH}_2$.^[23] Additional details regarding the protocols used for functionalization and high resolution transmission electron microscopy (HRTEM) images of the nanotubes are provided in the Supporting Information.

The required amount of functionalized MWNTs for the desired weight fraction was first weighed and dispersed in acetone (ratio of 1 mL of acetone to every 20 mg of nanotubes) with the help of a dispersion surfactant (BYK-9076 obtained from BYK Chemie Company). The mixture was stirred at 200 rpm for 15 min and then sonicated using a cup horn sonicator for 30 min. The mixture was added to Epoxy 2000 (bisphenol-A-based epoxy from Fibreglast Inc), stirred manually for 2 min, and then sonicated using a cup horn sonicator for a further 30 min. Degassing was then performed by heating the sample in a vacuum oven at 70°C for 10 h. This step was essential to evaporate and remove the acetone from the mixture. The sample was then cooled and 75 mg (0.5 wt%) of an air-releasing agent (BYK A-500) was added to the mixture. The mixture was stirred manually for 10 min and then degassed under vacuum at room temperature. Next, low viscosity curing agent 2120 obtained from Fibreglast Inc. was added and blended into the epoxy using a high-speed mixer, model ARE-250, from Thinky Corporation at 2000 rpm for 4 min. The mixture was then placed in vacuum again for a final degassing stage for 15 min. Then the mixture (nanotubes and epoxy) was poured into silicon molds. The composite was cured at room temperature and 90 psi pressure for 24 h, followed by 2 h of post cure at 90°C .

Fatigue crack propagation tests were conducted using a MTS-858 material testing system following ASTM standard E647-05. An initial pre-crack was created in the compact tension samples by gently tapping a fresh razor blade over a molded starter notch. The radius at the tip of the pre-crack was similar for

all the samples tested, which was confirmed by optical microscopy prior to testing. All tests were performed under load control at a constant load ratio R of 0.1 ($R = K_{\min}/K_{\max}$) and at a test frequency of 5 Hz. The crack length was measured using the compliance method and was confirmed by a high resolution video monitoring system.

The curing behavior of the epoxy composites was characterized with a modulated DSC (model Q1000, TA Instruments). A sample of approximately 5 mg was sealed in a hermetic aluminum pan. Dynamic scanning experiments were conducted at a ramp rate of $10\text{ }^{\circ}\text{C min}^{-1}$ from the ambient temperature to $250\text{ }^{\circ}\text{C}$ to obtain the curing heat-flow diagram of the composite. The cured sample was left in the DSC cell and cooled to room temperature under a controlled rate of $10\text{ }^{\circ}\text{C min}^{-1}$. The sample was reheated to $250\text{ }^{\circ}\text{C}$ at $10\text{ }^{\circ}\text{C min}^{-1}$ to obtain the second heat-flow diagram.

Keywords:

carbon nanotubes · crazing · epoxy nanocomposites · fatigue · toughness

-
- [1] J. G. Williams, *Fracture Mechanics of Polymers*, Ellis Horwood, Chichester **1984**.
- [2] A. J. Kinloch, R. J. Young, *Fracture Behavior of Polymers*, Applied Science Publishers, London **1983**.
- [3] H. R. Azimi, R. A. Pearson, R. W. Hertzberg, *Polym. Eng. Sci.* **1996**, *36*, 2352.
- [4] L. Becu, A. Maazouz, H. Sautereau, J. F. Gerard, *J. Appl. Polym. Sci.* **1997**, *65*, 2419.
- [5] A. J. Kinloch, J. G. Williams, *J. Mater. Sci.* **1980**, *15*, 987.
- [6] *Damage mechanics of composite materials* (Ed: R. Talrega), Elsevier, New York **1994**.
- [7] L. H. Lee, *Adhesive Bonding*, Plenum, New York **1991**.
- [8] W. Xu, S. Raychowdhury, D. D. Jiang, H. Retsos, E. P. Giannelis, *Small* **2008**, *4*, 662.
- [9] S. R. White, N. R. Sottos, P. H. Geubelle, J. S. Moore, M. R. Kessler, S. R. Sriram, E. N. Brown, S. Viswanathan, *Nature* **2001**, *409*, 794.
- [10] J. C. Radon, *Int. J. Fract.* **1980**, *16*, 533.
- [11] W. Zhang, R. C. Picu, N. Koratkar, *Appl. Phys. Lett.* **2007**, *91*, 193109.
- [12] W. Zhang, R. C. Picu, N. Koratkar, *Nanotechnology* **2008**, *19*, 285709.
- [13] W. Zhang, J. Suhr, N. Koratkar, *Adv. Mater.* **2006**, *18*, 452.
- [14] J. Suhr, W. Zhang, P. Ajayan, N. Koratkar, *Nano Lett.* **2006**, *6*, 219.
- [15] J. Suhr, N. Koratkar, P. Keblinski, P. Ajayan, *Nat. Mater.* **2005**, *4*, 134.
- [16] F. Erdogan, P. F. Joseph, *J. Am. Ceram. Soc.* **1989**, *72*, 262.
- [17] T. H. Courtney, *Mechanical Behavior of Materials*, McGraw Hill, Boston **2000**.
- [18] S. S. Sternstein, L. Ongchin, *Polym. Prepr.* **1969**, *10*, 1117.
- [19] S. Kohale, S. M. Molina, B. L. Weeks, R. Khare, L. J. Hope-Weeks, *Langmuir* **2007**, *23*, 1258.
- [20] M. S. Ozmusul, R. C. Picu, *Polymer* **2002**, *43*, 4657.
- [21] J. D. Wang, Y. F. Zhu, X. W. Zhou, G. Sui, J. Liang, *J. Appl. Polym. Sci.* **2006**, *100*, 4697.
- [22] T. Ramanathan, F. T. Fisher, R. S. Ruoff, L. C. Brinson, *Chem. Mater.* **2005**, *17*, 1290.
- [23] T. Saito, K. Matsushige, K. Tanaka, *Phys. B* **2002**, *323*, 280.

Received: December 18, 2008
Revised: January 24, 2009
Published online: March 19, 2009